Journal of Earth Science, *Vol. 33*, *No. 4*, *p. 901−915*, *August 2022* *ISSN 1674-487X*
Printed in China
https://doi.org/10.1007/s12583-021-1488-x

Microfracture Characterization in Sandstone Reservoirs: A Case Study from the Upper Triassic of Syria's Euphrates Graben

Ibrahem Yousef*, Vladimir Morozov, Vladislav Sudakov, Ilyas Idrisov
Institute of Geology and Petroleum Technologies, *Kazan Federal University*, *Kazan* 420111, *Russia*
Yousef Ibrahem: https://orcid.org/0000-0001-9295-4597; Morozov Vladimir: https://orcid.org/0000-0002-9713-2805;
Sudakov Vladislav: https://orcid.org/0000-0002-6865-7477; Idrisov Ilyas: https://orcid.org/0000-0002-7434-4055

ABSTRACT: The Euphrates Graben is located in eastern Syria. The Upper Triassic Mulussa F Formation sandstones serve as the primary reservoir intervals in the majority of the graben fields. The study's findings were based on core studies: petrographic examination of thin sections, scanning electron microscope (SEM), imaging of backscatter scanning electron microscope (BSE), X-ray microprobe examinations, and carbon-oxygen stable isotope analysis of microfracture-filling cements. Three of the most common types of microfracture found in the investigated sandstones are intragranular or intracrystalline microfractures, grain boundary or grain-edge microfractures, and transgranular (crossing grains) microfractures. Sandstone microfractures that are open and free of secondary mineralization improve sandstone storage and permeability. However, microfractures that are cemented and filled with secondary mineralization reduce storage and permeability. Common siderite and pyrite cements were identified within the microfractures and the nearby sandstone matrix. Larger anhedral or euhedral siderites are thought to form during shallow burial diagenesis, whereas poikilotopic siderites are thought to form during deep burial diagenesis. Poikilotopic pyrite is believed to be a diagenetic cement, which is attributed to the reduction of iron oxides present in the sediments in the presence of hydrocarbons. Microfractures reflect tectonic, overpressure, and diagenetic origins. Microfractures of tectonic origin are associated with folding and thrust activities over the Euphrates Graben area, and they were formed at the beginning of the Upper Triassic with siderite and pyrite cement equilibration temperatures of approximately 100–105 ºC, and they continued forming from the middle to the end of the Upper Triassic with cement equilibration temperatures of approximately 90–100 ºC in conjunction with the first phase of the Euphrates Graben. Microfractures related to diagenetic and overpressure processes are tension microfractures and were formed in compression settings during the Upper Triassic.
KEY WORDS: microfracture, sandstone, Upper Triassic, Mulussa F, Euphrates Graben, Syria.

0 INTRODUCTION

Natural occurring fractures in hydrocarbon reservoirs are common and important as fluid flow conduits and repositories of oil and gas (Anders et al., 2016). The large-scale fractures (macrofractures), they are usually studied directly from core samples or using imaging tools, for example, the formation microimager (FMI) and/or ultrasonic borehole imager (UBI) (Ameen and Hailwood, 2008). The microscopic fractures (microfractures) are studied using laboratory techniques, for example, polarizing and/or scanning electron microscopes (Bisdom et al., 2016).

The aims of this research are the following: (1) microfracture types and characteristics from the point of size, shape, patterns, and mode, (2) microfractures cement fills characteristics, (3) evolution of the diagenetic origins of the cement that fills the microfractures, (4) timing and origins of the microfractures, and (5) microfractures' influences on porosity.

The research is necessary since the economic production of the hydrocarbons in the siliciclastic reservoir rocks of the Mulussa F Formation depends sometimes on the characteristics of the naturally occurring microfractures, which are very important channels for fluid flow and accumulation and lead to an increase in the reservoir storage and production rates. Also, characterization of the microfractures can be used as paleostress indicators, strain gauges, and in providing evidence for the temperature of fracturing, fluid conditions, and timing. Such studies in petroleum geology are needed and important since they can provide key evidence of the processes of compaction, consolidation, growth, and development of the fault zones that govern the patterns of fluid flow within the sandstones of the Mulussa F Formation. Therefore, understanding

*Corresponding author: ibrahem.youseef@mail.ru

Manuscript received August 5, 2020.
Manuscript accepted May 27, 2021.

Yousef Ibrahem, Morozov Vladimir, Sudakov Vladislav, Idrisov Ilyas, 2022. Microfracture Characterization in Sandstone Reservoirs: A Case Study from the Upper Triassic of Syria's Euphrates Graben. *Journal of Earth Science*, 33(4): 901−915. https://doi.org/10.1007/s12583-021-1488-x. http://en.earth-science.net

the characterization, formation, and distribution of the microfractures has significance for natural gas exploration and development in the Euphrates Graben fields.

The novelty of the research is that characterization of the microfractures within the Mulussa F Formation sandstones continues to challenge geoscientists in the Euphrates Graben fields, as they are very common and well developed due to the tectonic structure and complex diagenetic history of the graben area.

Sediments of the Mulussa F Formation were studied in terms of sedimentology by (Ibrahem et al., 2022, 2021a, b; Yousef et al., 2021a, b, 2020, 2019, 2018a, b; Yousef and Morozov, 2017a, b), and this study is the first one related to microfracture characterization and is a continuation of the previous studies on the Mulussa F Formation in the Euphrates Graben. Results of the research can be beneficial for hydrocarbon activities in the fields of the Euphrates Graben area since the microfractures within the sandstone of the Mulussa F Formation are likely a key factor for controlling the hydrocarbon flow, accumulations, production rates, and changes in the reservoir properties.

1 SAMPLING AND ANALYTICAL PROCEDURES

The studied sandstone samples were collected from the reservoir intervals of the Mulussa F Formation in 12 wells distributed over the graben area as shown in Fig. 1c.

Detailed investigations and petrographic observations were performed on the sandstone full-length core intervals and on the selected thin section samples. The modal compositions were obtained from 40 representative sandstone samples by counting 300 points in each thin section. Thirty sandstone samples were examined using a backscatter scanning electron microscope (BSE) and a scanning electron microscope (SEM). Data interpretations of the UBI imaging tool in one well were also used for fracture distribution and azimuths. Stable carbon

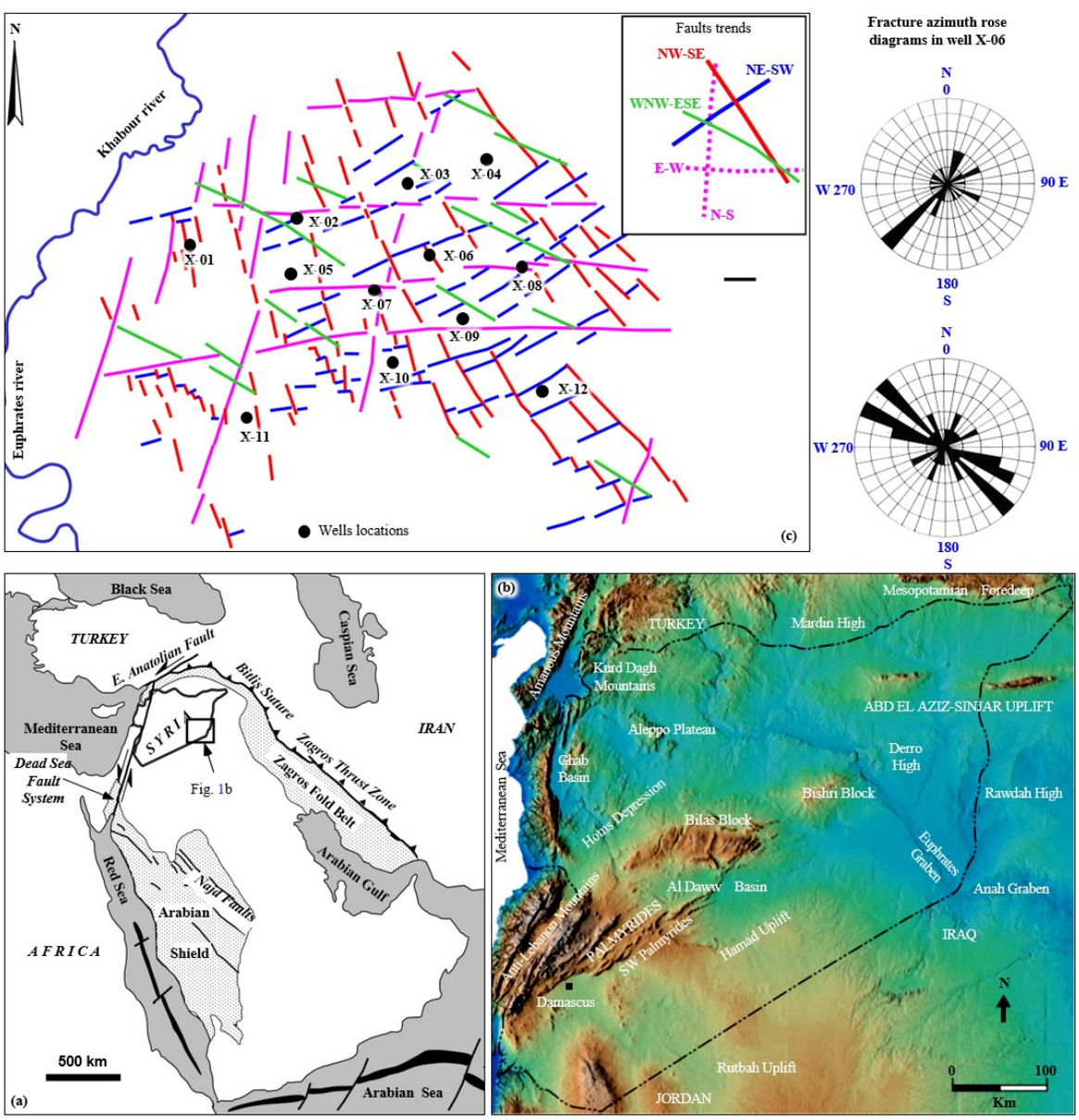

Figure 1. (a) Simplified map illustrates the tectonic settings of the Arabian Plate (Litak et al., 1998); (b) location map of the Euphrates Graben in Syria (Brew et al., 2000); (c) simplified map showing the different faults trends across the Euphrates Graben area.

and oxygen isotope analyses were carried out on 5 siderite-cemented sandstone samples. The equilibration temperature (ET) (ºC) calculated using the formula: $ET = 0.04 \times (\delta^{13}O)^2 - 4.548 \times (\delta^{18}O) + 23.85$(PDF) (Zuo et al., 2018).

2 GEOLOGIC SETTING

2.1 Structural Framework

The Euphrates Graben (Fig. 1b) is located in the eastern part of Syria, which is located on the northwestern slope of the Arabian plate (Fig. 1a), (Litak et al., 1998). The main tectonic blocks in Syria, which recorded uplifts and subsidence, include the Palmyrides, Euphrates Graben, Khleissia, and Sinjar-Abd El Aziz uplifts (Fig. 1b). The Euphrates Graben is the studied area and is one of the most important oil and gas basins in Syria (Ibrahem et al., 2021a, b). The 160-km-long Euphrates Graben is an intracratonic rift basin formed by the crustal extension during the Middle to Late Cretaceous Period(Yousef and Morozov, 2017a, b). The rift basin of the Euphrates Graben is characterized by a complex pattern of highly interlocking faults, according to different trends. Differential subsidence is predominantly controlled by the faults (Figs. 2a, 2b).

Most of the faults cut the Triassic and Cretaceous strata, some of which extended to cut the Cenozoic strata, others extended to cut the Paleozoic strata (Figs. 2a, 2b). Several independent hydrocarbon reservoirs were identified in the Euphrates Graben area, ranging in age from the Paleozoic to the Mesozoic, with the Triassic and Cretaceous reservoirs being the most important (Yousef et al., 2018a; Barrier et al., 2014). The combined information from the various data sources allows a subdivision of the fault families across the Euphrates Graben area into five major trends. The main orientations are color-coded (Fig. 1c).

The west-north-west to east-south-east WNW-ESE trends are similar to the general trend of the Euphrates Graben area (Fig. 1b). They reflect the fault elements which are perpendicular to the extension axis of the graben. Faults according to this trend control the major subsidence of the Euphrates Graben (Fig. 2b).

The north-west to south-east trends NW-SE, which are also similar to the general trend of the Euphrates Graben, are

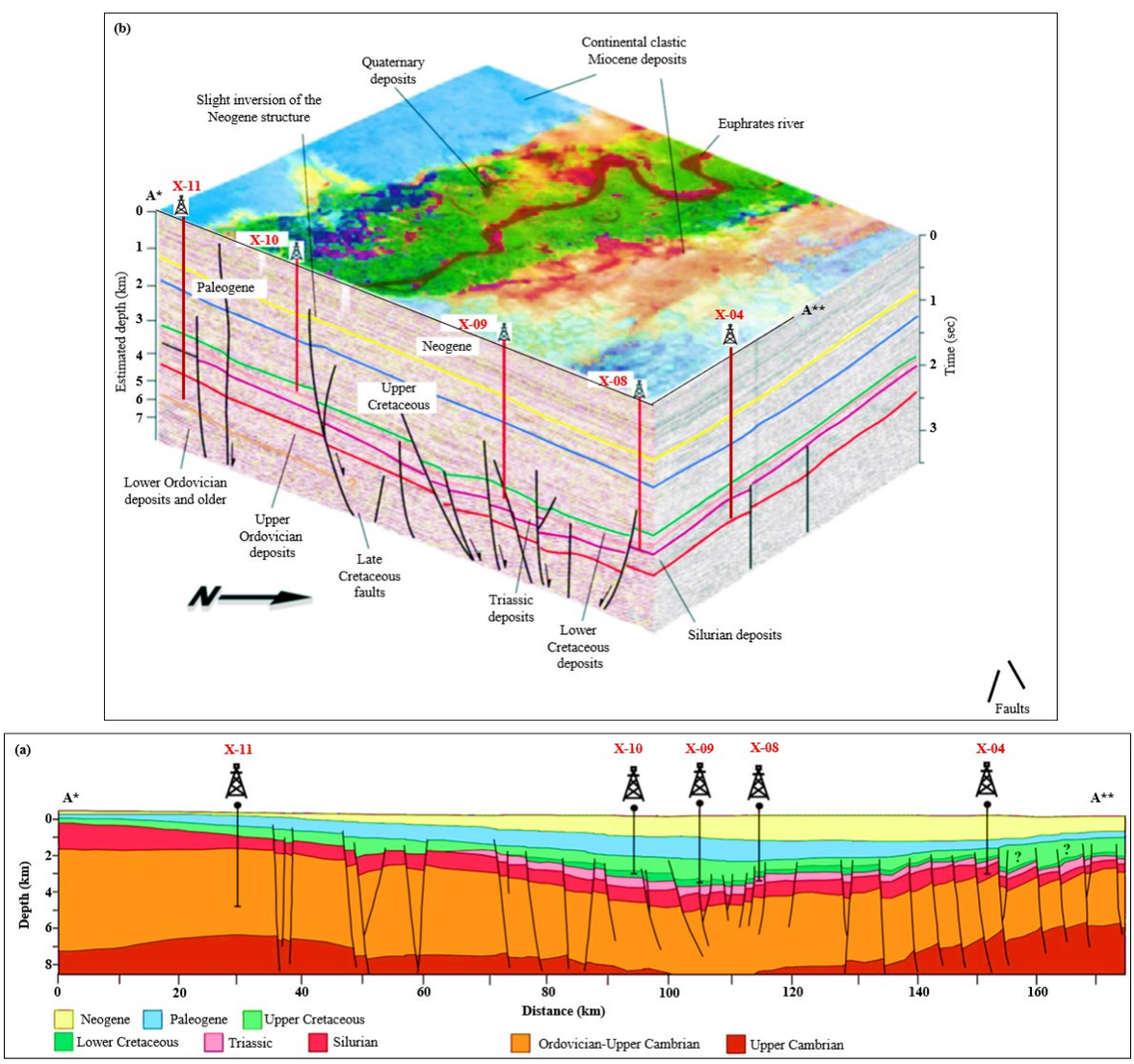

Figure 2. (a) 3D model of the Euphrates Graben based on seismic interpretation (Brew et al., 2000); (b) structural geological cross-section (A*–A**) across the Euphrates Graben area (Litak et al., 1998).

common over the Euphrates Graben area (Fig. 1c). The trends of these faults are associated with the WNW-ESE fault trends but have been diverted towards the northeast as a result of the Euphrates Graben Movement clockwise to the northeast under the influence of the Palmyrides compaction (Litak et al., 1997).

The northeast to southwest fault trends, which are parallel to the general trend of the Palmyrides, are also common over the Euphrates Graben area (Fig. 1c). These faults are generally considered an extension of the Palmyrides fold belt faults, but they were cut in the area of the Euphrates Graben by the WNW-ESE and the NW-SE faults. Additionally, there are also north-south and east-west fault trends over the Euphrates Graben. These faults are common and extend for long distances through the graben area, and are sometimes interrupted or cut by other faults with the trends mentioned above (Fig. 1c).

2.2 Stratigraphy and Sedimentology

Stratigraphically, the studied section covers the Upper Triassic Mulussa F Formation in the selected area in the Euphrates Graben area where its clastic sediments vary in thickness from 350 to 450 m and consist mainly of fluviatile channel sandstone bodies (10 to 60 m in thickness) with interbreeds of floodplain claystone (3 to 20 m in thickness) (Figs. 3a, 3b).

The regional stratigraphically information (Ibrahem et al., 2021a, b; Yousef et al., 2019, 2018a, b) indicates that sediments of the Mulussa F Formation over the Euphrates Graben area were influenced by the erosion accompanying with the regional base Early Cretaceous unconformity (BKL), (Fig. 3a), which resulted in varying thicknesses of the sediments over the fields of the Euphrates Graben area. Sediments of the Upper Triassic Mulussa F Formation are overlined by sediments of the Early Cretaceous Rutbah Formation, the BKL Unconformity separate between them as shown in Fig. 3a.

2.3 Reservoir Attributes

The sandstone bodies of the Mulussa F Formation are the main reservoir units over the Euphrates Graben area (Yousef et al., 2019). The source rocks are believed to be the deeper Triassic strata (Fig. 3a) (Syrian Petroleum Company, 1981). The reservoir lithology of the Mulussa F Formation is generally comprised of moderately to well-sorted, fine to medium to coarse-grained quartz arenites that vary in size from 250 to 500 µm with about 3% to 10% clay content (Figs. 4a, 4b, 4e) and have experienced weak to moderate degrees of compaction (Figs. 4b, 4e). The majority of the sandstones are texturally mature, with a framework assemblage consisting almost exclusively of detrital quartz.

Detrital feldspars vary from traces to about 5% with an average of 1% (based on point counting data). They include K-feldspar and plagioclase. Most of the feldspars were dissolved during the diagenesis, which led to generating secondary porosity, which developed the reservoir quality of the studied sandstone. The sandstones of the Mulussa F Formation, in general, are classified as quartz arenite (Fig. 4c), with the exception of

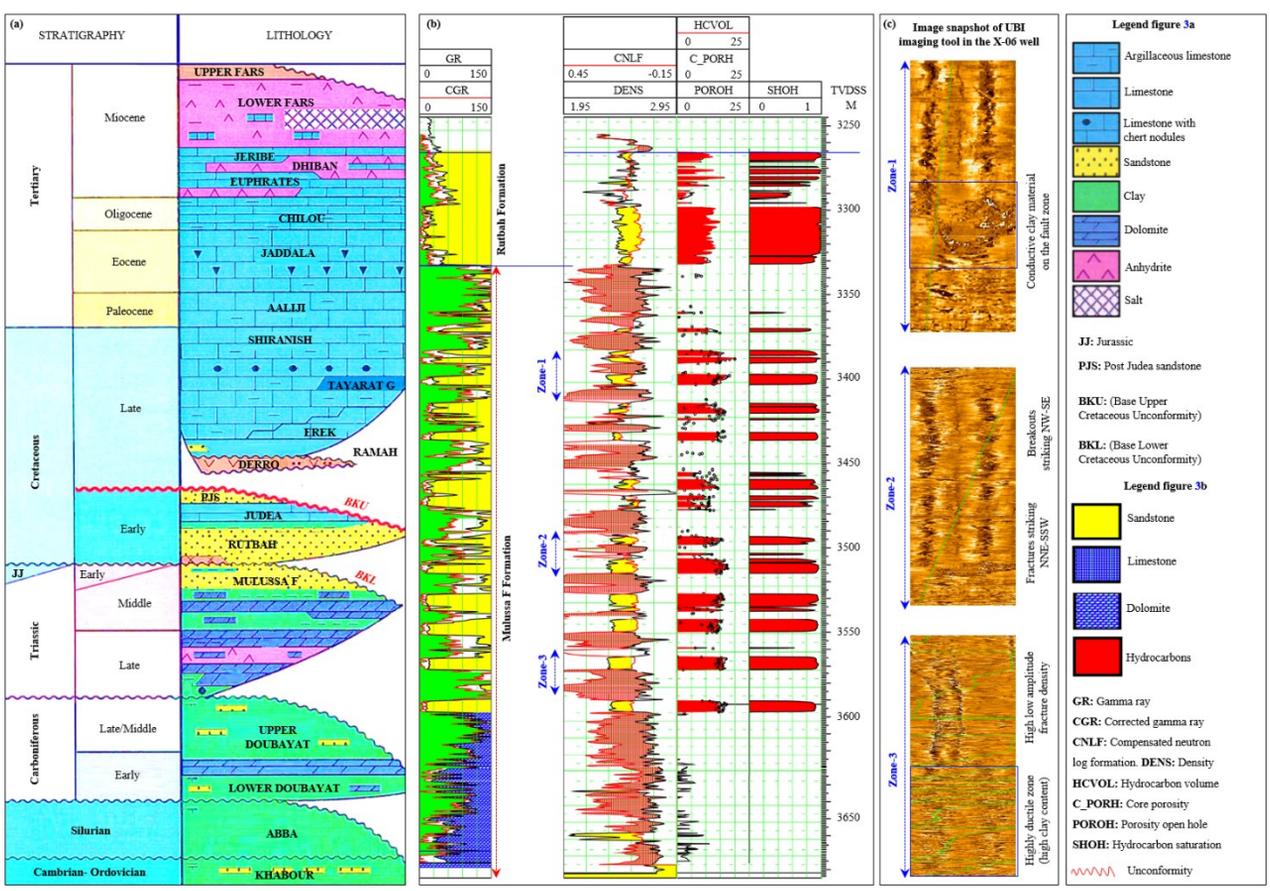

Figure 3. (a) General stratigraphic section of Euphrates Graben (Litak et al., 1998); (b) typical of the X-06 well logging response of Mulussa F Formation; (c) image snapshot of UBI imaging tool in the X-06 well. See Fig. 1c for the X-06 well location.

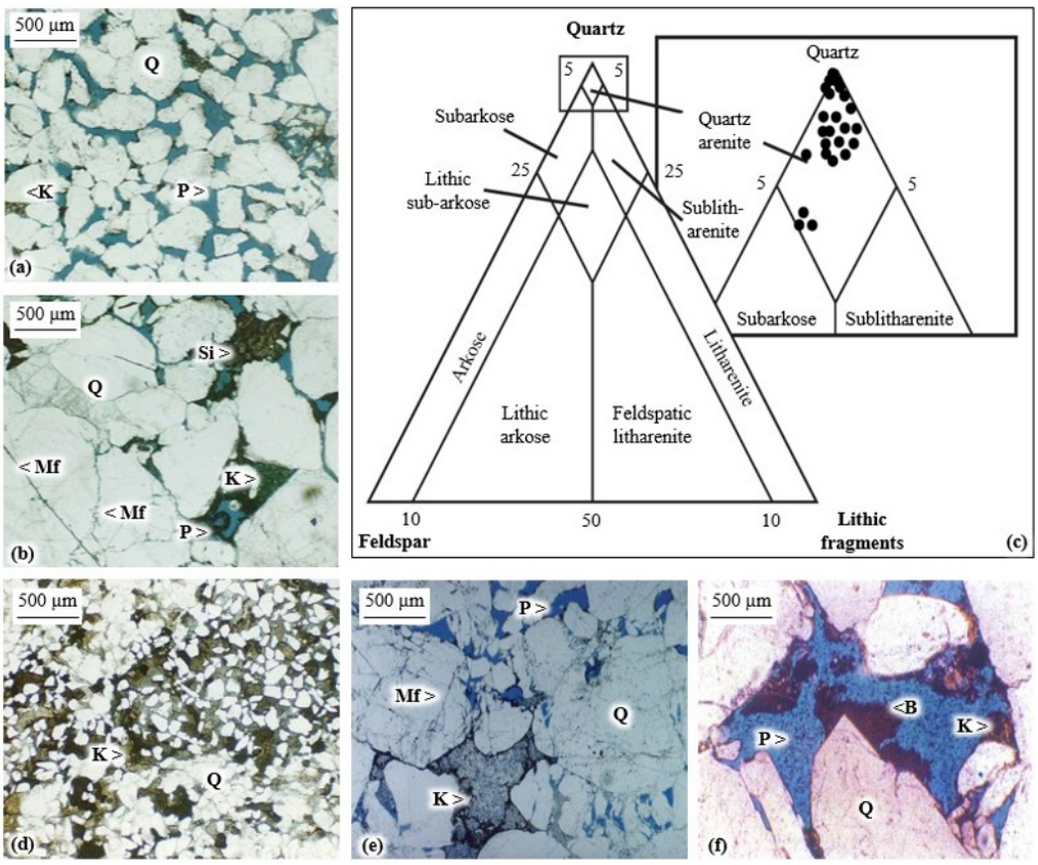

Figure 4. Representative optical photomicrographs. (a) Medium grained quartz arenite with low clay content; (b) coarse-grained quartz arenite with moderate degrees of compaction; (c) the framework grain composition of the representative sandstone samples from the Upper Triassic Mulussa F Formation plotted on McBride's (1963) classification; (d) very fine to fine-grained to quartz wackes; (e) Fractured quartz arenite, traces of kaolinite within some pores; (f) coarse-grained quartz arenite with secondary dissolution porosity. Abbreviations on photomicrographs: P. Pore; Q. quartz; Si. siderite; K. kaolinite; Mf. microfracture; B. bitumen.

some samples, which contain an excess of 25% detrital matrix clay and are therefore classified as quartz wackes (Fig. 4d). The sandstone thickness of the Mulussa F Formation varies between 35% and more than 70% of that of the gross stratum (Yousef et al., 2019). The burial depth of the Mulussa F Formation sediments over the fields of the Euphrates Graben is up to 3 700 m of true vertical depth subsea (TVDSS) (Yousef et al., 2018a).

The reservoir quality of the Mulussa F Formation sandstone according to well log interpretations as shown in Fig. 3b is generally good. The average total porosity from well logs is about 12%, with a range from 0.2% to 20%. As shown in Fig. 3b, the oil saturation values of the sandstone reservoir layers calculated from the well logs are up to 1%. The clay mineral content between the detrital components of the Mulussa F Formation sandstone is the main factor in controlling the reservoir properties. Additionally, the type and distribution of the secondary authigenic cement/minerals between the grains also affect the reservoir quality (Yousef et al., 2020; Yousef and Morozov, 2017a, b).

3 RESULTS AND DISCUSSION

3.1 Microfracture Morphology

Both open and sealed microfractures have been identified throughout the sandstone cored intervals. Induced fractures and microfractures, whether caused by drilling or caused by core handling, are not discussed here because they are artificial and cannot be interpreted as naturally occurring. The three main categories of microfractures were recognized in the thin sections of the studied sandstone samples based on the relationship between the microfractures and the quartz grains (Figs. 5a, 5b, 5c) (Hooker et al., 2013; Batzle et al., 1980; Simmons and Richter, 1976). These include: (1) the intragranular or intracrystalline microfractures that are lying totally within the quartz grains (Fig. 5a), (2) the grain boundary or grain-edge microfractures that are along the grain boundaries (Fig. 5b), and (3) the transgranular (traversing grain) microfractures that are across the grains or are across the grains from the grain boundaries (Fig. 5c).

3.1.1 Intragranular or intracrystalline microfractures

The examination of thin sections with transmitted light microscopy revealed that intragranular or intracrystalline microfractures are the most common type in coarse-grained sandstone samples; they are less common in fine- to medium-grained sandstone samples. Typically, they are identifiable as well-marked lines in the form of irregular arrays lying entirely within the quartz grains and the cleavage microfractures in the feldspars (Figs. 6a, 6b). Locally, the intragranular microfrac-

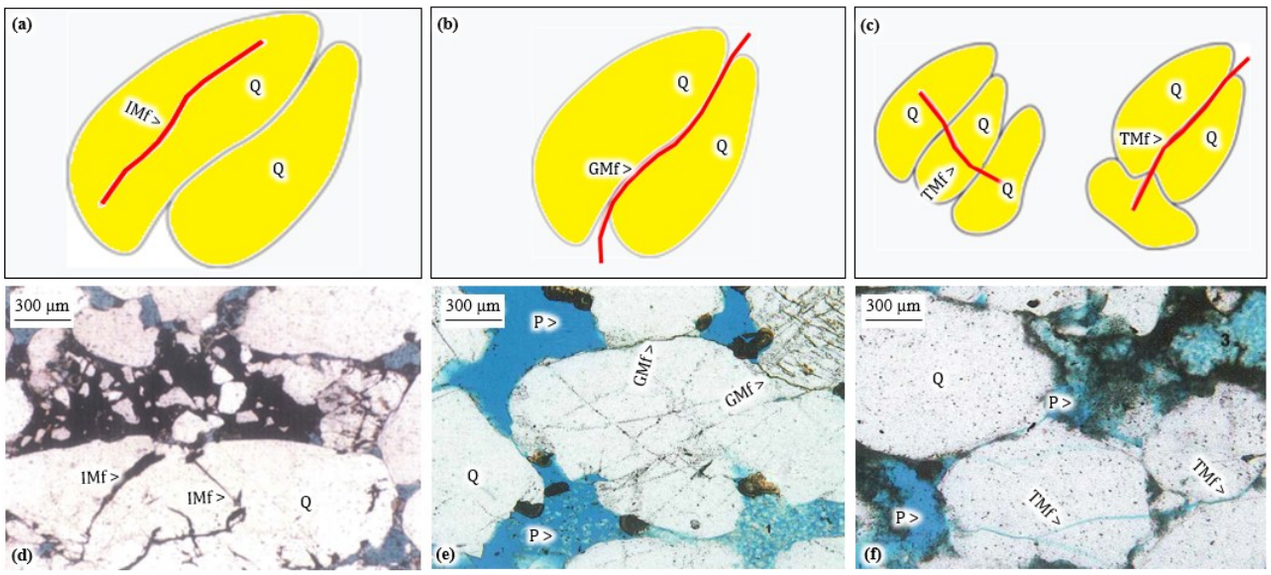

Figure 5. Grain-scale illustration of microfracture categories within sandstones of the Mulussa F Formation. (a) Intragranular or intracrystalline microfracture; (b) grain boundary or grain-edge microfracture; (c) transgranular (traversing grain) microfracture, representative optical photomicrographs showing; (d) quartz arenite, fine to coarse-grained, intragranular microfracture within some crystals; (e) quartz arenite, coarse-grained, grain-edge microfracture within some crystals; (f) quartz arenite, coarse-grained, transgranular microfracture within some crystals. Abbreviations on photomicrographs: P. Pore; Q. quartz; IMf. intragranular microfracture; GMf. grain-edge microfracture; TMf. traversing microfracture.

tures are relatively small in size, usually much less than the detrital quartz grain diameter in length and about 1 µm or less in width. They could be curved to straight traces arranged in a simple and/or complex intersecting pattern, and usually, they are not cut through the edge of the grains. The intragranular microfractures have high densities (Figs. 6a, 6b). Other intragranular microfractures lack secondary mineral deposits (Fig. 6c). The lines of the microfractures are traceable from one grain to another by thin strings of these secondary minerals. In contrast, thermally or mechanically induced intragranular microfractures have sharp walls, are generally narrow, and typically lack secondary mineral deposits. Based on sandstone grain textural relations, it is suggested that the intragranular microfractures within sandstones of the Mulussa F Formation were formed mainly before or during the early stages of the quartz grain cementation processes. This is consistent with the local medium to large displacements of the fractured grains on both sides of the microfracture (Figs. 6a, 6c, arrows).

3.1.2 Grain boundary or grain-edge microfractures

The grain boundary or grain-edge microfractures are usually narrow in width and short in length. They have varying degrees of aperture range between 10 and 20 µm, although they have experienced dissolution and a few of them could reach up to 80 µm or longer (Figs. 6d, 6e). The grain-edge microfractures are associated and may be coincident with the grain boundaries along linear contacts so that they can also be called intergranular microfractures (Fig. 6f).

Grain boundary or grain-edge microfractures may be subdivided into those coincident with and non-coincident with the actual crystal boundary (Simmons and Richter, 1976). It is often difficult to make this distinction because the grain boundary may not be obvious. Non-coincident grain boundary microfractures may extend for short distances into the grain at a high angle to the grain boundary (Fig. 6f), or may be close to and subparallel to the boundary, possibly running through the grain boundary asperities or adjacent cementation materials (Fig. 6g). Coincident grain boundary microfractures are separations (open space) between part or all of the crystal boundary and the adjacent cementation materials (Fig. 6h).

3.1.3 Transgranular (traversing grain) microfractures

The term transgranular (traversing grain) microfractures is sometimes used for microfractures running across a grain from grain boundary to grain boundary. The transgranular microfractures are usually wider and longer, and their length is not restricted by the size of the grains. They could have straight traces or inclined across many grains (Fig. 6k) and/or across one grain (Fig. 6k, arrows). The short transgranular microfractures (less than 40 µm) extend across the single grain (Fig. 6k, arrows), while the longer transgranular microfractures (typically are greater than 100 µm and less than 10 µm wide) cut across and cut several tens of the grain and/or grain boundaries and the intervening cement without having any consistent relation to grain centers or grain contacts (Figs. 6k, 6l). In several samples, the transgranular microfractures have the morphology of secondary (authigenic) crystals growing within the space of the fracture (Figs. 6m, 6n).

In some cases, the transgranular microfractures end at the grain boundaries or subdivide the grains into multiple grains (Fig. 6m, arrows). These patterns show that the transgranular microfractures grew after the formation of cementation materials between the grains. Some of the transgranular microfractures are widened by the dissolution of the grains and/or cements. Therefore, they can increase the connectivity in otherwise ultralow-permeability reservoir rocks.

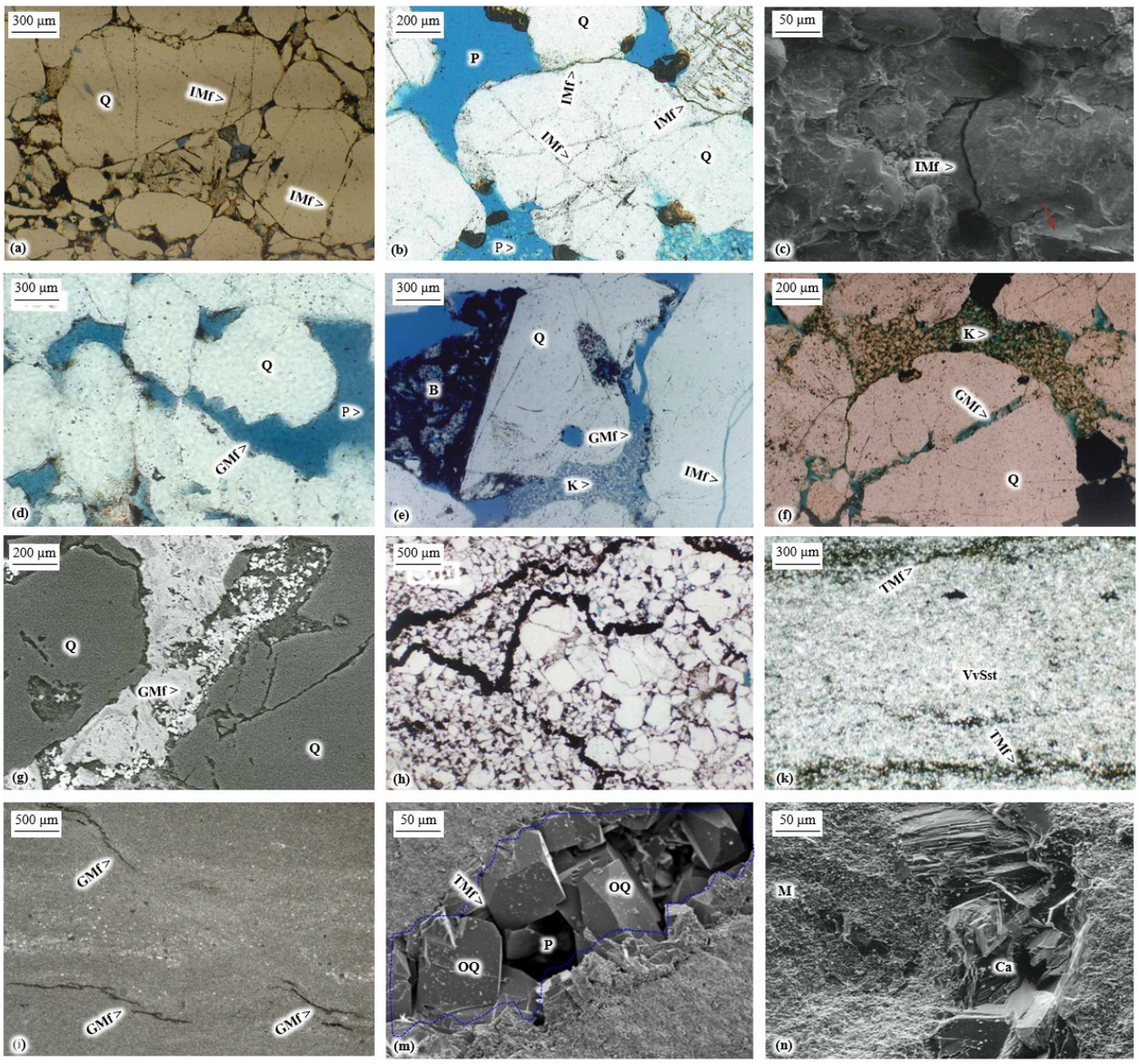

Figure 6. Representative optical and SEM photomicrographs. (a), (b) Intragranular microfractures in quartz grains; (c) intragranular microfractures, SEM; (d) experienced dissolution open grain-edge microfracture along the boundary of quartz grain; (e) experienced dissolution grain-edge microfracture along the boundary of quartz grain, intragranular microfractures also excited; (f) grain-edge microfracture along the boundary of quartz grain, SEM; (g), (h) traversing grain microfracture in the very fine to coarse-grained sandstone, some of the microfractures are cemented and sealed by the secondary authigenic minerals; (k) traversing grain microfracture across the very fine sandstones; (l) traversing grain microfracture, (arrows) in the medium-grained sandstone; (m) authigenic quartz within microfracture zone, SEM; (n) authigenic calcite within microfracture zone, SEM. Abbreviations on photomicrographs: Q. Quartz; K. kaolinite; IMf. intragranular microfracture; GMf. grain-edge microfracture; TMf. traversing microfracture; M. micrite; Ca. calcite; OQ. overgrowth quartz; P. pore; B. bitumen; VvSst. very fine sandstone.

3.2 Microfractures Cementation

Sedimentological investigations have revealed significant microfracture zones within the sandstone intervals of the Mulussa F Formation (Fig. 3c). Some are open and uncemented (Figs. 7a, 7b), while others are partially or completely cemented and filled with siderite (Figs. 7c, 7d, 7e, 7g), pyrite (Fig. 7f), kaolinite (Fig. 6k), or authigenic quartz (Fig. 6m).

In this paragraph, we will discuss siderite and pyrite as microfracture cementation materials since they are the main filling materials within the microfracture. Other cements, for example, kaolinite, quartz, and calcite, will not be discussed because they exist as traces between the detrital components of the Mulussa F Formation sandstones and do not have any significant effects on the reservoir properties. In general, pyrite cement is considered less common in the sandstone of the Mulussa F sediments compared to siderite cement.

The microfracture zone shown in Figs. 7c and 7d is severely cemented by brecciated siderite (Figs. 7e, 7g), and subsequent late pyrite (Fig. 7f), although their distribution varies within the microfracture zone. Both pyrite and siderite are composed of non-isometric grains distributed in the primary pores and in/or along the microfracture zones and vary in size from

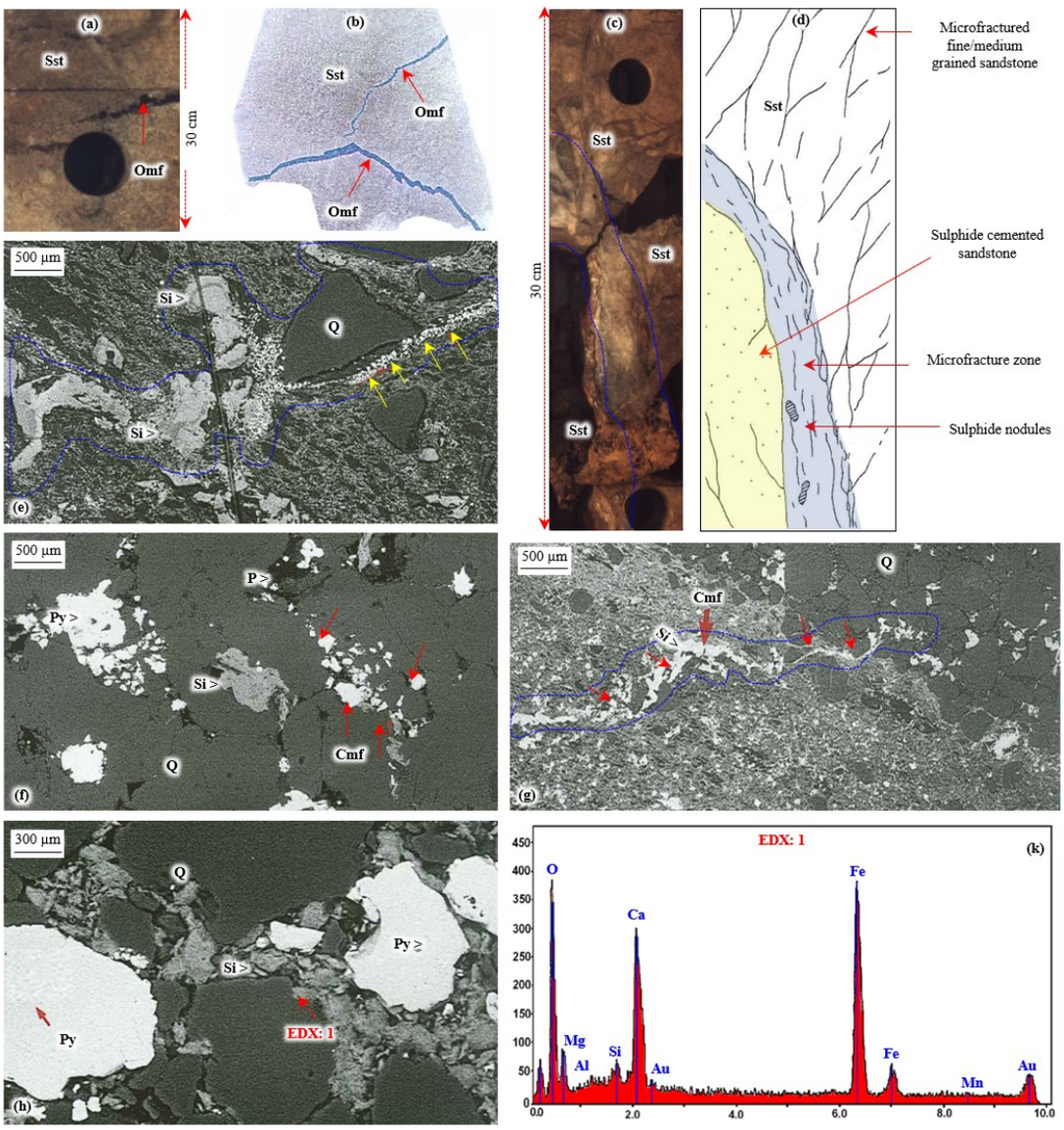

Figure 7. (a) Representative core photography showing open microfracture; (b) photomicrographs of the thin section showing open microfracture zone; (c), (d) core sketch of cemented microfracture zone; (e) siderite-cemented microfracture, the siderite is partially zoned (centre); (f) microfracture zone characterized by siderite, pyrite blocks postdate and replace siderite; (g) narrow, linear siderite-cemented microfracture zone (arrowed); (h) pyrite blocks occupy the intergranular pores; (k) point EDX analysis of siderite. Abbreviations on photomicrographs: Sst. Sandstone; Omf. open microfracture; Si. Siderite; Q. quartz; P. pore; Py. pyrite; Cmf. closed microfracture.

20 µm or smaller up to 200 µm. Both these phases have migrated into the adjacent sandstone matrix to a minimal detected distance of 5 cm, reducing the effective porosity within the microfracture-proximal parts of the matrix (Figs. 7e, 7g). Within part of the siderite-cemented microfracture (Fig. 7e), the siderite is partially zoned (center), reflecting the variations in the Ca-Fe pore fluid content (Baker et al., 1996). Disseminated pyrite (Fig. 7e, arrows), possibly partially replacing earlier siderite, has also developed within the microfracture zone. This suggests later sulphide-rich fluid also used this route for access into the adjacent sandstone porosity. In the primary pores within the adjacent matrix (Fig. 7f), pyrite cement is accompanied by siderite (light grey-center) cement. This is post-dated and partially replaced by a subsequent pyrite invasion.

The sandstone-mudstone contact (Fig. 7g) is penetrated by a narrow, linear zone of siderite cement (arrows). This microfracture allowed CO_2-rich fluids to penetrate the sandstone intergranular porosity and precipitate siderite (bright phase in BSE). The lower part of the fracture zone (Fig. 7h) is characterized by early siderite blocks, which line the framework surfaces and are post-dated by pyrite (brighter intensity) cement, suggesting a subsequent influx of sulphide fluids (Morad, 1998). In some situations, the pyrite appears to replace the siderite.

4 DISCUSSION

4.1 Origin of Cements

Although it is relatively difficult to determine the exact timing of the siderite cement in the sandstone of the Mulussa F Formation, the overall paragenetic sequence (Fig. 8) was established based on the textural relationships and oxygen isotopic

data, in addition to the available literature (Ibrahem et al., 2021a, b). Petrographic observations indicate that the siderite forms the major carbonate cement between the sandstone of the Mulussa F Formation and the different sizes of siderite (Fig. 7) suggest that it was formed under various diagenetic conditions (Morad, 1998).

It is likely that the smaller anhedral/euhedral siderite, which fills the smaller pores (Figs. 7e, 7f) and partially the sandstone matrix (Fig. 7g) and locally engulfs the kaolinite (Fig. 6f), occurred in the early stage of the diagenesis (Morad, 1998). Conversely, the larger poikilotopic siderite that fills large intergranular pores (Figs. 9a, 9b) and the microfracture spaces (Figs. 7e, 7g) in loosely packed framework grains is believed to be formed during deeper burial diagenesis conditions subsequently to the formation of pores and microfractures and before the rock was subjected to any compactional processes. What indicates this is that the distribution of siderite is usually flowing along the microfracture paths and the siderite crystals/cement did not show any morphological deformation processes (Figs. 9a, 9b).

The initial composition of the siderite is significantly affected by the magnesium concentration in the porous water (Mozley and Wersin, 1992). Based on the chemical analysis results, the smaller anhedral/euhedral siderite shows a magnesium-poor composition (between 0.1% and 3.2%), which indicates its precipitation from the meteoric pore waters. Conversely, the larger poikilotopic siderite with high magnesium concentrations (up to 25%) indicates its precipitation from the high magnesium concentration pore waters (Morad et al., 2010; Wilson et al., 2003).

The presence of siderites within the matrix and microfractures of the Mulussa F Formation sandstones probably reflects the mobilisation of iron under organic-rich reducing conditions. Coal bands indicate that organic matter was locally abun-

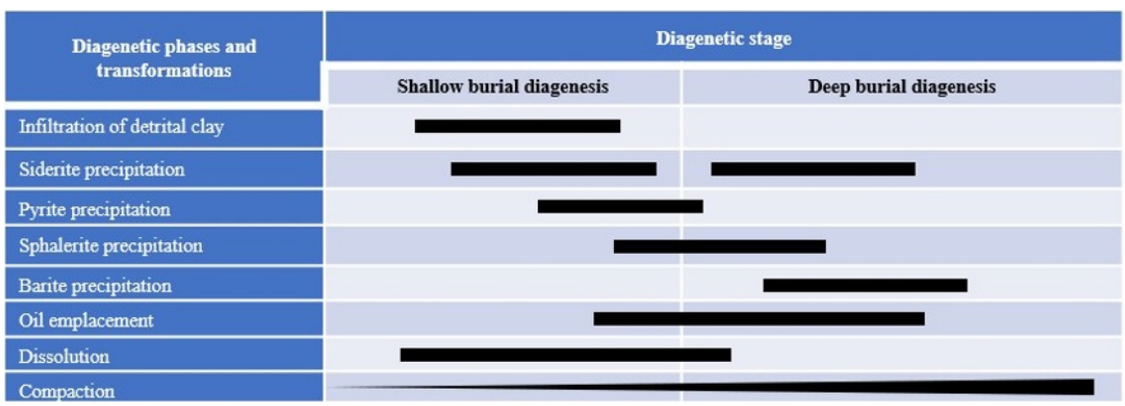

Figure 8. The diagenetic sequence of the Mulussa F Formation in the Euphrates Graben area. Data are from Ibrahem et al. (2021a, b).

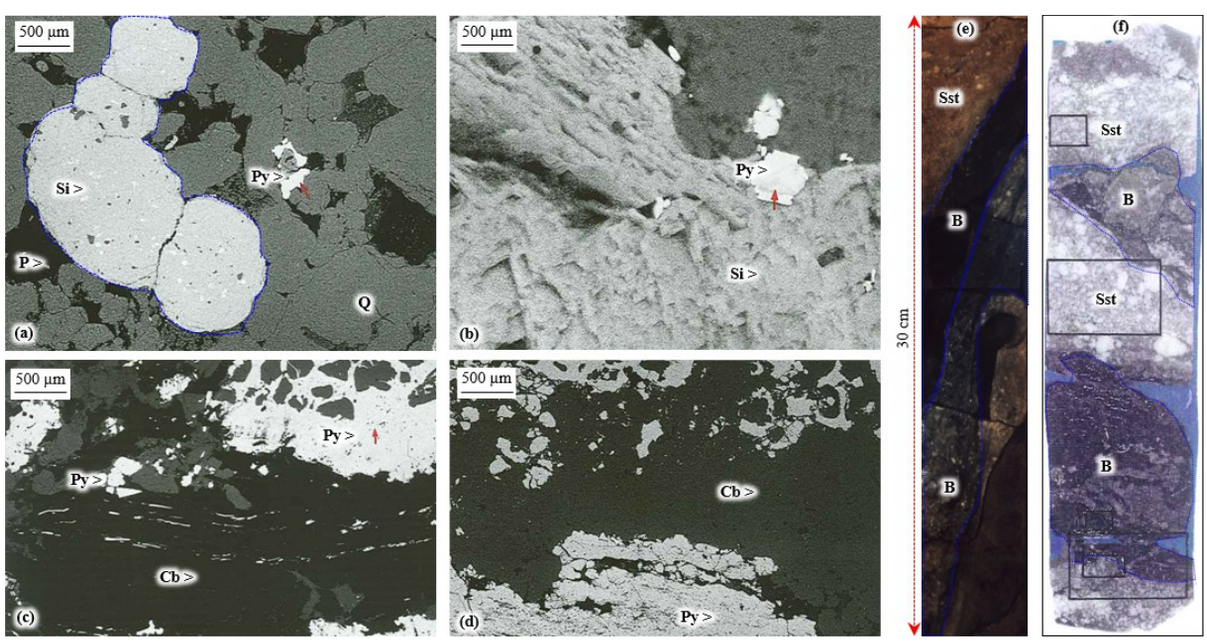

Figure 9. Representative BSE images. (a) Subspherical siderite replacing the unstable grains, pyrite cement developed within the pore network; (b) siderite within the primary porosity; (c), (d) an organic-rich coal band (black) has acted as an effective slippage plane during fracturing. Pyrite cement form linear streaks within the coal (centre) and large composite aggregates (top right). The latter disrupts the framework of grain fabric; (e) representative core photograph showing microfracture zone filled with bitumen; (f) core sketch of microfracture zone filled with bitumen. Abbreviations on photomicrographs: Si. Siderite; Py. Pyrite; Q. quartz; Cb. coal bands.

dant within sediments of the Mulussa F Formation (Figs. 9c, 9d). Bacterial processes within the substrate probably influenced the formation of siderite spherulites (Fig. 9a) by progressively removing all oxygen and SO_4^{-2} sulphate ions, or by reducing ferric iron to ferrous iron, or by raising the pH (Mozley and Wersin, 1992).

Pyrite cement is a minor cement identified within the sandstone of the Mulussa F Formation. Two forms of pyrite cement were recognized; the first one is the framboidal pyrite, which is found as scattered invasions within the microfractures and partially within the matrix (Figs. 7f, 9a). The second type of pyrite is the poikilotopic, which is composed of very large crystalline, sub-anhedral in shape, growing and filling the intergranular voids (Fig. 9h), supporting the quartz framework grains (Fig. 9c) and replacing part of the coal bands (Fig. 9d). This explains why this pyrite had a major role in severe porosity reduction. The framboidal pyrite cement results from the microbial activity within the sediments in which the resulted H_2S initiates pyritization processes in the organic matter bearing mudstones. In those parts of the floodplain (where the Mulussa F Formation sediments were deposited) that lacked freshwater circulation, oxygen rapidly became depleted and anaerobic bacterial processes commenced. Scattered pyrite crystals possibly record the reduction and removal of sulphate ions before ferric iron reduction began (Anders et al., 2014; Raiswell, 1982). The massive poikilotopic pyrite cement is believed to be a diagenetic cement, which is attributed to the reduction of the iron oxides present in the sediments in the presence of hydrocarbons (Kalliokoski, 1966). The earliest fluids were CO_2-rich, suboxic, with high Fe activity. Subsequent fluids were reduced to S-rich but retained high Fe activity.

4.2 Microfractures Origin and Timing

The previously described microfractures are widely present in the sandstones of the Mulussa F Formation. They are non-filled to partially or totally filled with siderite or pyrite (Figs. 7, 8), and sometimes they are filled with calcite (Fig. 6n) or overgrowth quartz (Fig. 6m). Three origins of the microfractures within the sandstones of the Mulussa F Formation were identified, including the microfractures of tectonic origin, the microfractures of overpressure origin, and the microfractures of diagenetic origin (Wilson et al., 2003; Kranz, 1983). On the basis of analyzing the overlapping relations of the authigenic minerals within the microfractures, fluid inclusions of the microfractures and their cement fill (Ju et al., 2017; Padovani et al., 1982), the timing of the microfractures was deduced.

(a) Microfractures of tectonic origin

Within the sandstone of the Mulussa F Formation, microfractures of tectonic origin are most commonly present. Most of the transgranular microfractures have tectonic origins. Based on thin section examinations (Figs. 6, 7, 9), the tectonic microfractures are usually distinguished by their length. Generally, they are long, and have a regular distribution within the sandstone texture. They are part of the same macrofractures populations that are associated with the tectonic activity over the Euphrates Graben, including the folds and thrusts, since the graben area is characterized by very active tectonic activity over the eastern part of Syria (Litak et al., 1998, 1997).

The results of the BSE/SEM examinations showed that the siderite and pyrite cements were trapped within the microfractures during their precipitation (Figs. 7, 8). Some siderite and pyrite cements appear to have precipitated between the detrital sandstone components before any compaction activates subjected to the sandstones. This is based on the observations from the thin section examination where these cements show local morphological deformations resulting from crushing by the subsequent compaction (Figs. 7e, 7g). Additionally, some siderite and pyrite cements appear to have precipitated after the compression activates. This is evidenced by the fact that they occupy most of the microfractures and do not show any morphological deformations resulting from the subsequent compaction (Figs. 7h, 9a). The fluids responsible for siderite and pyrite cements were probably hydrothermal in origin, gaining access to the Mulussa F Formation through the tectonic faulting over the graben area (Fig. 2) and distributed as irregular strings or groups within the microfractures. The differences in the cement content suggest gradual changes in the pore fluid sources (Mozley, 1989).

Apatite fission track analysis (AFTA) showed that the estimated maximum post-dispositional temperature of the Upper Triassic sequence within the Euphrates Graben fields ranges from 100 to 105 ºC (Fig. 10). Based on oxygen stable isotope analysis of the microfractures siderite-filling cement (Table 1), these values are close to 91 to 99 ºC.

Based on the different observations and analyses, it is suggested that the microfractures tectonic event had two events: the first microfractures tectonic event formed during the deposition time of the Upper Triassic Mulussa F Formation sandstones with siderite and pyrite cement equilibration temperature range of approximately 100 to 105 ºC. This is based on the observations that showed that most of the microfractures are filled by the siderite and pyrite cements. Furthermore, these cements support the matrix and the framework of the detrital quartz grains. The second micro fracturing tectonic event is thought to have continued from the Upper Triassic to the beginning of the Early Cretaceous, with cement equilibration temperatures ranging from 90 to 100 ºC, with the Euphrates Graben rifting during the Early Cretaceous (Yousef et al., 2018b).

Table 1 Oxygen and carbon isotopes of the cements fill the microfractures of the Mulussa F Formation in the Euphrates Graben area

Well No.	Depth (m)	Lithology	$\delta^{13}C_{PDB}{}^{100}$	$\delta^{18}O_{PDB}{}^{100}$	Equilibration temperature (°C)
X-1	2 300	Fine sandstones	-3.9	-16.8	99.6
X-3	2 180	Fine sandstones	-2.7	-15.0	91.7
X-4	2 250	Fine sandstones	-2.8	-15.2	92.6
X-6	2 330	Fine sandstones	-3.4	-16.3	97.06
X-8	2 498	Fine sandstones	-3.2	-16.5	98.4

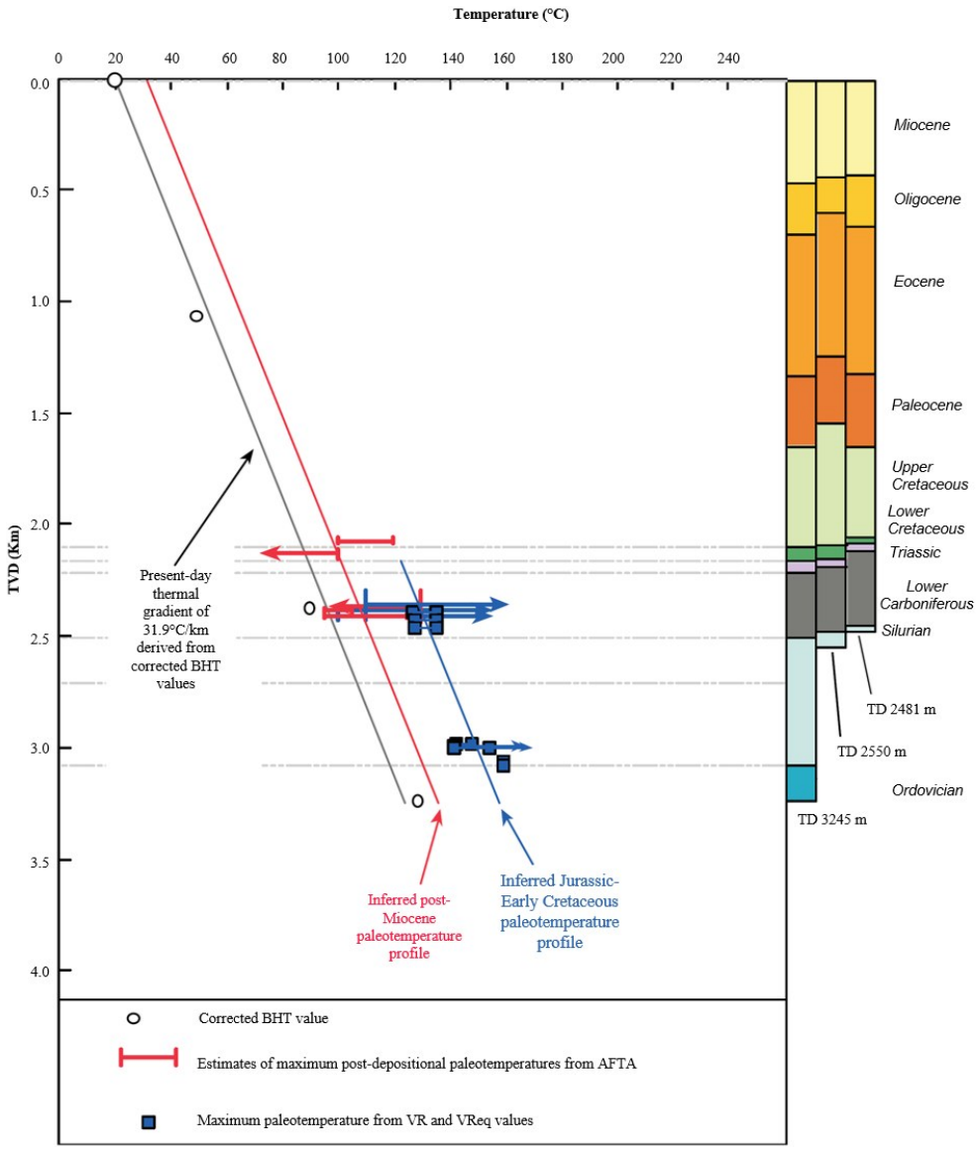

Figure 10. Burial and geo-temperature history of the Upper Triassic Mulussa F Formation in the Euphrates Graben area.

(b) Microfractures of overpressure origin

Some of the microfractures in the sandstone of the Mulussa F Formation were interpreted as overpressure-originated microfractures. This is based on observations from the petrographic study of the thin section, which showed that some of these microscopic fractures are associated with veins filled with organic-rich or coal bands (Figs. 9c, 9d), or they may contain bitumen (Figs. 9e, 9f). Based on the available literature about the structural history of the Euphrates Graben (Yousef et al., 2018a; Yousef and Morozov, 2017a; Litak et al., 1998, 1997), the compaction started during the Upper Triassic and reached its peak at the end of the Cretaceous, and this coincided with the subsidence phases that the depression was exposed to (Fig. 2b). Compaction led to the generation of many fractures and/or macrofractures in the Upper Triassic sediments as well as the Cretaceous sediments over the stratigraphical strata of the Euphrates Graben area.

Compaction events over the Euphrates Graben have also resulted from the regional stress events associated with the movement of the Arabian tectonic plate (Fig. 1a) towards the northwest, in addition to the stress applied to the graben area from the Palmyra fold zone to the west and southwest of the Euphrates Graben (Brew et al., 2000; Litak et al., 1997). All these factors combined have led to increased compaction and stress in the graben area. The decrease in the pore fluid pressure values below the static pressure values of the upper layers/strata led to the closure of most of the microfractures and/or their filling with calcite cement as shown in Fig. 6n.

(c) Microfractures of diagenetic origin

Diagenetic microfractures are defined as those formed during the diagenesis processes (Shu et al., 2020; Wilson et al., 2003). They can be transgranular microfractures, intragranular microfractures, and/or grain-edge microfractures. The transgranular (traversing grain) microfractures of diagenetic origin are present in the sandstones of the Mulussa F Formation mainly on the boundaries between the sandstone and the mudstone parallel to sub-parallel to the bedding as shown in Fig. 11a.

They are well developed along microlayers and especially

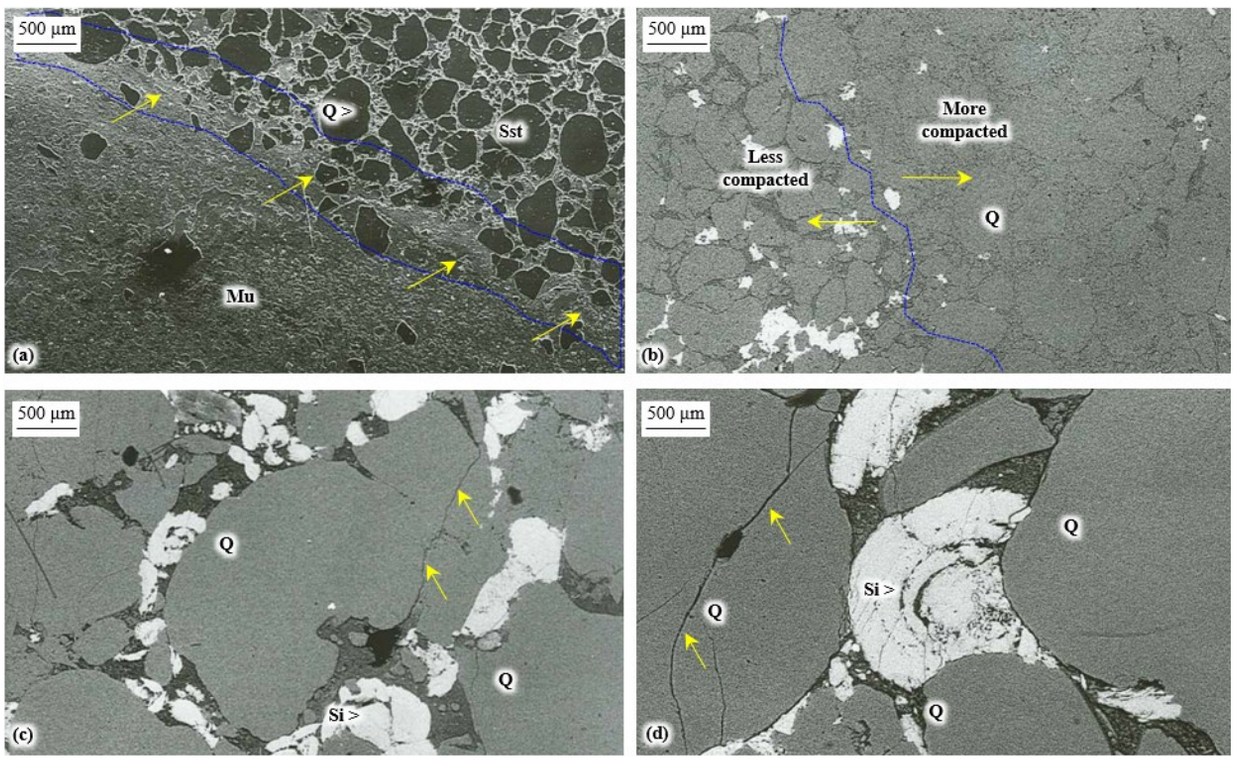

Figure 11. Representative BSE images. (a) Microfractures presented on the boundaries between sandstone and mudstone and cemented with clay materials; (b) compacted sandstones (right), less compacted (lift); (c), (d) intragranular or intracrystalline and grain boundary or grain-edge microfractures within the sandstones, siderite also excited in some intergranular pores. Abbreviations on photomicrographs: Si. Siderite; Q. quartz; Mu. mudstone; Sst. sandstone.

in the argillaceous rocks, additionally, they are commonly cemented with the clay materials. The intragranular or intracrystalline microfractures and grain boundary or grain-edge microfractures are considered diagenetic microfractures because they were formed during the compaction processes that the sandstone was subjected to. Typically, grain boundary or grain-edge microfracture occurs in conjunction with intragranular or intracrystalline microfracture. In general, if the rocks were subjected to more compacting, then less debris will be presented between the grains and/or within the microfractures or the fractures (Figs. 11b, 6b, 6g). Additionally, as more the grains are rougher and are close to each other's in a linear pattern, the better opportunity is to develop the intragranular or intracrystalline microfractures and grain boundary or grain-edge microfractures (Figs. 11b, 11c). The intragranular or intracrystalline microfractures are mainly related to mechanical compaction (Fig. 11c). The grain boundary or grain-edge microfractures are primarily related to compaction and/or pressure solution (Figs. 6d, 6e). The diagenetic analyses of the Upper Triassic Mulussa F Formation suggest that the formation of the diagenetic origin microfractures was during and at the end of the Upper Triassic.

5 INFLUENCE OF MICROFRACTURES ON RESERVOIR QUALITY

Based on thin section examination, four main types of pores occur in the sandstones of the Mulussa F Formation, including: (1) the intergranular pores (Figs. 12b, 4a), (2) the solution-related pores (Figs. 12c, 12d, 12e, 4f), (3) the microfracture pores (Figs. 12f, 4b), and (4) the intercrystalline pores/non-effective porosity in the clay minerals (Figs. 4d, 4e). Of the four pore types, the open intergranular and the secondary (microfractures and/or dissolution) pores are the most significant in the storage and transmissibility of the fluids. Based on the petrophysical analyses of the core plugs, the porosity values of the sandstones of the Mulussa F Formation range from 1% up to 20%, with an average of 12% (Fig. 12a). The average total permeability is about 597 mD, with a range from 0.01 to 3 150 mD (Fig. 12a).

A cross plot of the relationship between the porosity and the permeability in Fig. 12a shows two groups of porosities: the first one where the porosities are up to 10%, and the second one where the porosities are from 10% up to 20%. Petrography investigation of the thin section shows that common porosities in the first group are the intergranular porosity, while in the second group are the secondary dissolution and/or the microfracture porosity in addition to the intergranular porosity (Figs. 12c, 12d, 12e, 12f). The secondary open pores resulted from the partial or complete leaching of the unstable grains and/or from the microfractures in the sandstone framework form up to 10% by volume according to point-count data. The pores are generally interconnected and effectively enhance permeability and transmissibility when connected with intergranular pores (Figs. 12c, 12d, 12e, and 12f). Secondary porosity is locally occluded by vermicular kaolinite (Fig. 6f).

Dissolution and fracture porosity significantly influence the reservoir quality of the Mulussa F sandstones (Figs. 12e, 12f, 6b, 6d, 6e, 6h). The interpretation of the UBI tool logs in the well X-06 (Fig. 3s) showed many fractured zones over the Mulussa F Formation interval. Most of the fractures are in the

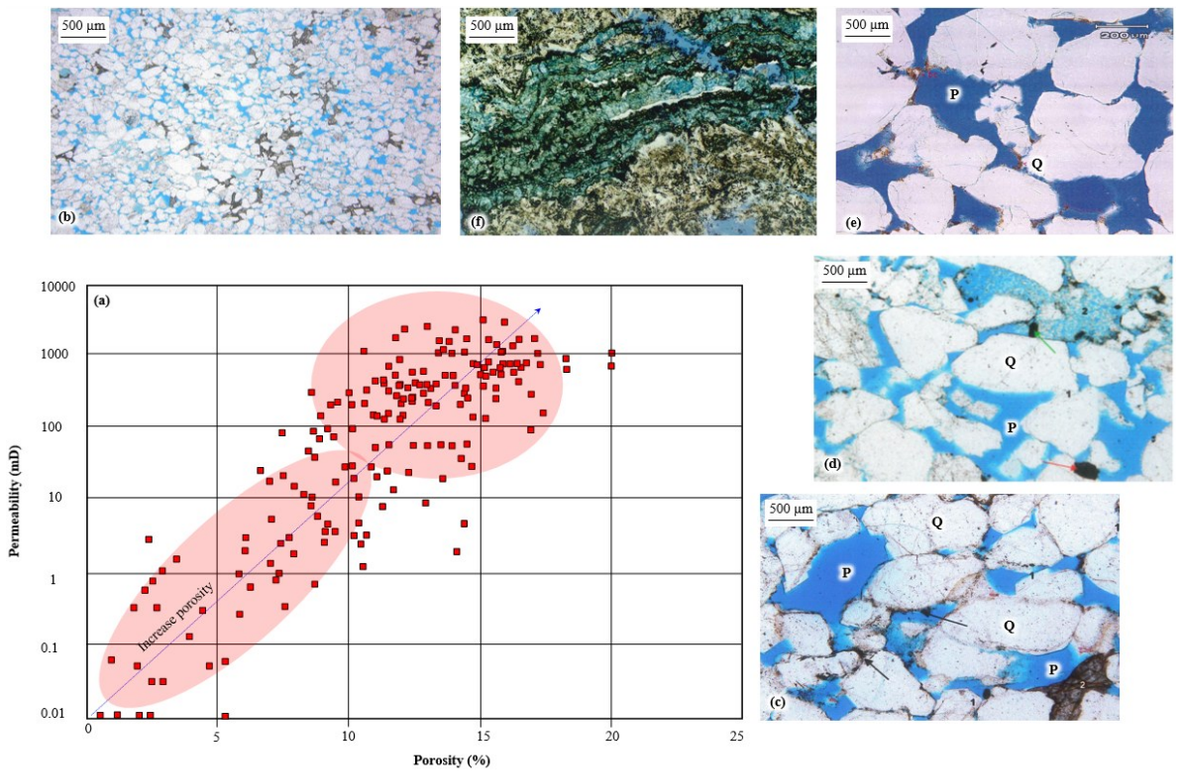

Figure 12. (a) Cross plot of porosity and permeability in the sandstones of the Mulussa F Formation; (b) intergranular porosity within fine granular sandstone; (c), (d), (e) secondary porosity with medium to coarse sandstones; (f) microfractures and dissolution porosity with sandstones.

NNE-SSW direction from comparing the oil saturation values in Fig. 3c with the fractured zones from the interpretation of the UBI tool, it's clear that the open fractures/microfractures contribute to enhancing the reservoir quality of the Mulussa F Formation sandstones.

6 CONCLUSIONS

Three types of microfractures have been distinguished within the sandstones of the Upper Triassic Mulussa F Formation in the Euphrates Graben fields based on different core materials investigations and analyses, this includes the intragranular or intracrystalline microfractures, the grain boundary or grain-edge microfractures, and the transgranular (traversing grain) microfractures. The intragranular and grain-boundary microfractures play a major factor in hydrocarbon storage due to their development at different structures within the sandstones and due to their small size and permeability. They were formed due to the crushing of the quartz grains under rapid sedimentation and intense compaction. Some of the microfractures are open-mode, they improve storage and permeability of the sandstones. Other microfractures are partially or completely filled-mode by secondary cements. The larger poikilotopic siderite cements that were distinguished within the microfractures and the adjacent sandstone matrix are believed to be formed in the deep burial diagenesis conditions, while the smaller siderites are believed to be formed in the shallow burial diagenesis conditions. The massive poikilotopic pyrite is believed to be a diagenetic cement, which is attributed to the reduction of the iron oxides present in the sediments in the presence of the hydrocarbons.

Microfractures within the sandstones reflect three origins; tectonic origin, overpressure origin, and/or diagenetic origin. Tectonic microfractures controlled by fold-thrust are developed within the studied sandstones and have the largest contribution to hydrocarbon production. They are believed to have been formed during the Upper Triassic with a siderite and pyrite cement equilibration temperature of approximately 90 to 105 ºC. Diagenetic microfractures are a result of the influence of compaction during the diagenetic processes. The microfractures related to overpressure origin have little contribution to hydrocarbon production due to their narrow diameters and cement fills. Microfracture and dissolution porosity play the main roles in developing the reservoir quality of the Mulussa F Formation over the studied area in the Euphrates Graben.

ACKNOWLEDGMENTS

This work was supported by the Ministry of Science and Higher Education of the Russian Federation under the agreement within the framework of the development program for a world-class research center "Efficient Development of the Global Liquid Hydrocarbon Reserves" (No. 075-15-2020-931). The authors are grateful to the reviewers and editors for their informative comments, which assisted in the interpretation of the findings and improved the article's quality. The final publication is available at Springer via https://doi.org/10.1007/s12583-021-1488-x.

REFERENCES CITED

Ameen, M. S., Hailwood, E. A., 2008. A New Technology for the Characterization of Microfractured Reservoirs (Test Case: Unayzah

Reservoir, Wudayhi Field, Saudi Arabia). *AAPG Bulletin*, 92(1): 31–52. https://doi.org/10.1306/08200706090

Anders, M. H., Laubach, S. E., Scholz, C. H., 2014. Microfractures: A Review. *Journal of Structural Geology*, 69: 377–394. https://doi.org/10.1016/j.jsg.2014.05.011

Baker, J. C., Kassan, J., Hamilton, P. J., 1996. Early Diagenetic Siderite as an Indicator of Depositional Environment in the Triassic Rewan Group, Southern Bowen Basin, Eastern Australia. *Sedimentology*, 43 (1): 77–88. https://doi.org/10.1111/j.1365-3091.1996.tb01461.x

Barrier, E., Machlour, L., Blaizot, M., 2014. Chapter 11: Petroleum Systems of Syria. In: Marlow, L., Kendall, C., Yose, L., Eds., Petroleum Systems of the Tethyan Region. *AAPG Memoir*, 106: 335–378. https://doi.org/10.1036/13431862m1063612

Batzle, M. L., Simmons, G., Siegfried, R. W., 1980. Microcrack Closure in Rocks under Stress: Direct Observation. *Journal of Geophysical Research Atmospheres*, 85(B12): 7072–7090. https://doi.org/10.1029/jb085ib12p07072

Bisdom, K., Bertotti, G., Nick, H. M., 2016. The Impact of *in-situ* Stress and Outcrop-Based Fracture Geometry on Hydraulic Aperture and Upscaled Permeability in Fractured Reservoirs. *Tectonophysics*, 690: 63–75. https://doi.org/10.1016/j.tecto.2016.04.006

Brew, G., Barazangi, M., Sawaf, T., et al., 2000. Tectonic Map and Geologic Evolution of Syria: The Role of GIS. *The Leading Edge*, 19 (2): 176–182. https://doi.org/10.1190/1.1438571

Hooker, J. N., Laubach, S. E., Marrett, R., 2013. Fracture-Aperture Size—Frequency, Spatial Distribution, and Growth Processes in Strata-Bounded and Non-Strata-Bounded Fractures, Cambrian Mesón Group, NW Argentina. *Journal of Structural Geology*, 54: 54–71. https://doi.org/10.1016/j.jsg.2013.06.011

Ibrahem, Y., Morozov, V. P., Sudakov, V., 2021a. Dolomitization of the Lower Cretaceous Carbonate Reservoir in the Euphrates Graben, Syria. *Petroleum Science*, 18(5): 1342–1356. https://doi.org/10.1016/j.petsci.2021.09.020

Ibrahem, Y., Morozov, V. P., El Kadi, M., et al., 2021b. Porosity Enhancement Potential through Dolomitization of Carbonate Reservoirs, a Case of Study from the Euphrates Graben Fields, East Syria. *Petroleum*, https://doi.org/10.1016/j.petlm.2021.05.005

Ibrahem, Y., Morozov, V. P., Sudakov, V., et al., 2022. Sedimentary Diagenesis and Pore Characteristics for the Reservoir Evaluation of Domanik Formations (Semiluksk and Mendymsk) in the Central Part of Volga-Ural Petroleum Province. *Petroleum Research*, 7(1): 32–46. https://doi.org/10.1016/j.ptlrs.2021.08.002

Ju, W., Wu, C. F., Wang, K., et al., 2017. Prediction of Tectonic Fractures in Low Permeability Sandstone Reservoirs: A Case Study of the Es3m Reservoir in the Block Shishen 100 and Adjacent Regions, Dongying Depression. *Journal of Petroleum Science and Engineering*, 156: 884–895. https://doi.org/10.1016/j.petrol.2017.06.068

Kalliokoski, J., 1966. Diagenetic Pyritization in Three Sedimentary Rocks. *Economic Geology*, 61(5): 872–885. https://doi.org/10.2113/gsecongeo.61.5.872

Kranz, R. L., 1983. Microcracks in Rocks: A Review. *Tectonophysics*, 100 (1/2/3): 449–480. https://doi.org/10.1016/0040-1951(83)90198-1

Litak, R. K., Barazangi, M., Beauchamp, W., et al., 1997. Mesozoic–Cenozoic Evolution of the Intraplate Euphrates Fault System, Syria: Implications for Regional Tectonics. *Journal of the Geological Society*, 154(4): 653–666. https://doi.org/10.1144/gsjgs.154.4.0653

Litak, R. K., Barazangi, M., Brew, G., et al., 1998. Structure and Evolution of the Petroliferous Euphrates Graben System, Southeast Syria. *AAPG Bulletin*, 82(6): 1173–1190. https://doi. org/10.1306/1d9bca2f-172d-11d7-8645000102c1865d

McBride, E. F, 1963. A Classification of Common Sandstones. *SEPM Journal of Sedimentary Research*, 33(3): 664–669. https://doi. org/10.1306/74d70ee8-2b21-11d7-8648000102c1865d

Morad, S., 1998. Carbonate Cementation in Sandstones: Distribution Patterns and Geochemical Evolution. Carbonate Cementation in Sandstones. Blackwell Publishing Ltd., Oxford. 1–26. https://doi.org/10.1002/9781444304893.ch1

Morad, S., Al-Ramadan, K., Ketzer, J. M., et al., 2010. The Impact of Diagenesis on the Heterogeneity of Sandstone Reservoirs: A Review of the Role of Depositional Facies and Sequence Stratigraphy. *AAPG Bulletin*, 94(8): 1267–1309. https://doi.org/10.1306/04211009178

Mozley, P. S., 1989. Relation between Depositional Environment and the Elemental Composition of Early Diagenetic Siderite. *Geology*, 17(8): 704–706. https://doi. org/10.1130/0091-7613(1989)0170704: rbdeat>2.3.co;2

Mozley, P. S., Wersin, P., 1992. Isotopic Composition of Siderite as an Indicator of Depositional Environment. *Geology*, 20(9): 817–820. https://doi.org/10.1130/0091-7613(1992)0200817:icosaa>2.3.co;2

Padovani, E. R., Shirey, S. B., Simmons, G., 1982. Characteristics of Microcracks in Amphibolite and Granulite Facies Grade Rocks from Southeastern Pennsylvania. *Journal of Geophysical Research*: *Solid Earth*, 87(B10): 8605–8630. https://doi.org/10.1029/JB087iB10p08605

Raiswell, R., 1982. Pyrite Texture, Isotopic Composition and the Availability of Iron. *American Journal of Science*, 282(8): 1244–1263. https://doi.org/10.2475/ajs.282.8.1244

Simmons, G., Richter, D., 1976. Microcracks in Rock. In: Strens, R. G. J., Ed., The Physics and Chemistry of Minerals and Rocks. Wiley, New York. 105–137

Shu, L., Shen, K., Yang, R. C., et al., 2020. SEM-CL Study of Quartz Containing Fluid Inclusions in Wangjiazhuang Porphyry Copper (-Molybdenum) Deposit, Western Shandong, China. *Journal of Earth Science*, 31(2): 330–341. https://doi.org/10.1007/s12583-019-1025-3

Syrian Petroleum Company (SPC), 1981. On the Status of Hydrocarbon Exploration in Syrian Arab Republic during 1971–1980. Hydrocarbon Exploration Seminar. Organization of Arab Petroleum Exporting Countries, Kuwait. 91–121

Wilson, J. E., Chester, J. S., Chester, F. M., 2003. Microfracture Analysis of Fault Growth and Wear Processes, Punchbowl Fault, San Andreas System, California. *Journal of Structural Geology*, 25(11): 1855–1873. https://doi.org/10.1016/S0191-8141(03)00036-1

Yousef, I., Morozov, V., 2017a. Characteristics of Upper Triasic Sandstone Reservoirs in Syria Using Analysis of Laboratory Methods. *Georesursy*, 19(4): 356–363. https://doi.org/10.18599/grs.19.4.8

Yousef, I., Morozov, V., 2017b. Structural and Mineralogical Characteristics of the Clay Minerals in Upper Triassic Sandstone Reservoir, Euphrates Graben, East Syria. *Neftyanoe Khozyaystvo*, (8): 68–71. https://doi.org/10.24887/0028-2448-2017-8-68-71

Yousef, I., Morozov, V., El Kadi, M., 2020. Influence and Control of Post-Sedimentation Changes on Sandstone Reservoirs Quality, Example, Upper Triassic (Mulussa F Reservoir), and Lower Cretaceous (Rutbah Reservoir), Euphrates Graben, Syria. *Russian Journal of Earth Sciences*, 20(2): 1–24. https://doi.org/10.2205/2020es000706

Yousef, I., Morozov, V., Sudakov, V., et al., 2021a. Cementation Characteristics and Their Effect on Quality of the Upper Triassic, the Lower Cretaceous, and the Upper Cretaceous Sandstone Reservoirs, Euphrates Graben, Syria. *Journal of Earth Science*, 32(6): 1545–1562.

https://doi.org/10.1007/s12583-020-1065-8

Yousef, I., Morozov, V., El Kadi, M., et al., 2021b. Tectonic and Erosion Features, and Their Influence on Zonal Distribution of the Upper Triassic and the Lower Cretaceous Sediments in the Euphrates Graben Area, Syria. *Geodynamics and Tectonophysics* 12(3): 608–627. https://doi.org/10.5800/gt-2021-12-3-0541

Yousef, I., Shipaeva, M., Morozov, V., et al., 2019. Lithofacies Analysis and Depositional Environments of the Upper Triassic and Lower Cretaceous Sediments in Euphrates Graben Syria. 19th SGEM International Multidisciplinary Scientific GeoConference EXPO Proceedings. 279–286. https://doi.org/10.5593/sgem2019/1.1

Yousef, I., Sudakov, V., Morozov, V., et al., 2018a. Diagenetic Clay Minerals and Reservoir Quality of the Upper Triassic Sandstone in Euphrates Graben, East of Syria. International Multidisciplinary Scientific GeoConference Surveying Geology and Mining Ecology Management, SGEM 18(1.4). 397–404. https://doi.org/10.5593/sgem2018/1.4/s06.052

Yousef, I., Sudakov, V., Morozov, V., et al., 2018b. Structural Setting and Zonal Distribution of Upper Triassic–Lower Cretaceous Reservoirs in the Syrian Euphrates Graben. International Multidisciplinary Scientific GeoConference Surveying Geology and Mining Ecology Management, SGEM, 18(1.4). 811–818. https://doi.org/10.5593/sgem2018/1.4

Zuo, J. X., Peng, S. C., Qi, Y. P., et al., 2018. Carbon-Isotope Excursions Recorded in the Cambrian System, South China: Implications for Mass Extinctions and Sea-Level Fluctuations. *Journal of Earth Science*, 29 (3): 479–491. https://doi.org/10.1007/s12583-017-0963-x